

On the Connection between Supermassive Black Hole and Galaxy Growth in the Reionization Epoch

JUNYAO LI,^{1,2,3} JOHN D. SILVERMAN,^{2,4} TAKUMA IZUMI,^{5,6} WANQIU HE,⁵ MASAYUKI AKIYAMA,⁷ KOHEI INAYOSHI,⁸
YOSHIKI MATSUOKA,⁹ MASAFUSA ONOUE,^{8,2} AND YOSHIKI TOBA^{10,11,9}

¹*CAS Key Laboratory for Research in Galaxies and Cosmology, Department of Astronomy, University of Science and Technology of China, Hefei 230026, China*

²*Kavli Institute for the Physics and Mathematics of the Universe (WPI), The University of Tokyo, Kashiwa, Chiba 277-8583, Japan*

³*School of Astronomy and Space Science, University of Science and Technology of China, Hefei 230026, China*

⁴*Department of Astronomy, School of Science, The University of Tokyo, 7-3-1 Hongo, Bunkyo, Tokyo 113-0033, Japan*

⁵*National Astronomical Observatory of Japan, 2-21-1 Osawa, Mitaka, Tokyo 181-8588, Japan*

⁶*Department of Astronomical Science, Graduate University for Advanced Studies (SOKENDAI), 2-21-1 Osawa, Mitaka, Tokyo 181-8588, Japan*

⁷*Astronomical Institute, Tohoku University, Aramaki, Aoba, Sendai 980-8578, Japan*

⁸*Kavli Institute for Astronomy and Astrophysics, Peking University, Beijing 100871, China*

⁹*Research Center for Space and Cosmic Evolution, Ehime University, 2-5 Bunkyo-cho, Matsuyama, Ehime 790-8577, Japan*

¹⁰*Department of Astronomy, Kyoto University, Kitashirakawa-Oiwake-cho, Sakyo-ku, Kyoto 606-8502, Japan*

¹¹*Academia Sinica Institute of Astronomy and Astrophysics, 11F of Astronomy-Mathematics Building, AS/NTU, No.1, Section 4, Roosevelt Road, Taipei 10617, Taiwan*

ABSTRACT

The correlation between the mass of supermassive black holes (SMBHs; \mathcal{M}_{BH}) and their host galaxies (\mathcal{M}_{\star}) in the reionization epoch provides valuable constraints on how their growth are jointly assembled in the early universe. High-redshift quasars typically have a $\mathcal{M}_{\text{BH}}/\mathcal{M}_{\star}$ ratio significantly elevated in comparison to the local value. However, it is unclear by how much this apparent offset is driven by observational biases for the most distant quasars. To address this issue, we model the sample selection and measurement biases for a compilation of 20 quasars at $z \sim 6$ with host properties based on ALMA observations. We find that the observed distribution of quasars in the $\mathcal{M}_{\text{BH}} - \mathcal{M}_{\star}$ plane could be fully reproduced by assuming that the underlying SMBH populations at $z \sim 6$ follow the relationship in the local universe. However, a positive or even a negative evolution in $\mathcal{M}_{\text{BH}}/\mathcal{M}_{\star}$ can also explain the data, depending on how the intrinsic scatter evolves and the strength of various systematic uncertainties. This imposes critical requirements on improving the accuracy of mass measurements and expanding the current sample to lower \mathcal{M}_{BH} limits to break degeneracies. Interestingly, quasars that are significant outliers in $\mathcal{M}_{\text{BH}}/\mathcal{M}_{\star}$ tend to move towards the local relation given their instantaneous BH accretion rate and star formation rate. This may provide tentative evidence that a self-regulated SMBH–galaxy coevolution scenario is already in place at $z \sim 6$, with AGN feedback being a possible driver.

Keywords: Active galactic nuclei (16) — Quasars (1319) — Supermassive black holes (1663) — AGN host galaxies (2017) — Galaxy Evolution (594)

1. INTRODUCTION

Active galactic nuclei (AGN) or quasars, powered by mass accretion onto SMBHs, produce an enormous amount of energy that has been long-specified to have profound impacts on galaxy evolution (e.g., King & Pounds 2015). In the local universe, the mass of SMBHs

appears to be closely connected to the bulge properties (e.g., bulge mass $\mathcal{M}_{\text{bulge}}$, stellar velocity dispersion σ_{\star}), which inspired the concept of “coevolution” in studies of SMBH and galaxy evolution (e.g., Kormendy & Ho 2013).

High-redshift studies have mainly focused on the $\mathcal{M}_{\text{BH}} - \mathcal{M}_{\star}$ relation, with mounting evidence showing that its evolution in massive systems is not significant since $z \sim 2$ (e.g., Jahnke et al. 2009; Schramm & Silverman 2013; Sun et al. 2015; Ding et al. 2020; Li et al.

2021). In particular, its intrinsic scatter appears similar to the local value (e.g., [Ding et al. 2020](#); [Li et al. 2021](#)). These results suggest that a physical coupling (e.g., AGN feedback) between SMBHs and galaxies is likely at work to keep $\mathcal{M}_{\text{BH}}/\mathcal{M}_\star$ relatively constant. To decipher how the relationship was first established in the early universe, a key strategy would be to measure the $\mathcal{M}_{\text{BH}} - \mathcal{M}_\star$ relation in the reionization era ($z > 6$) where we are able to probe the first generation of accreting SMBHs (e.g., [Inayoshi et al. 2020](#)).

Many of the $z \sim 6$ quasars discovered so far are powered by extremely massive BHs with $\mathcal{M}_{\text{BH}} \sim 10^9 M_\odot$ (e.g., [Fan et al. 2000](#); [Shen et al. 2019](#)), and are actively forming stars with star formation rates (SFR) $\sim 100 - 1000 M_\odot \text{ yr}^{-1}$ (e.g., [Wang et al. 2013](#)). Their $\mathcal{M}_{\text{BH}}/\mathcal{M}_\star$ (where \mathcal{M}_\star is approximated by the dynamical mass \mathcal{M}_{dyn} measured from gas kinematics using ALMA) appears to be significantly offset from the local value by up to 2.0 dex, suggesting that the growth of SMBHs substantially precedes their hosts (e.g., [Neeleman et al. 2021](#)). However, these quasars are biased tracers of the underlying SMBH populations, as only the most luminous quasars powered by the most massive BHs can be detected in shallow surveys (e.g., [Lauer et al. 2007](#); [Volonteri & Stark 2011](#); [Schulze & Wisotzki 2014](#)). The fact that lower-luminosity quasars detected in deeper surveys (e.g., the SHELLQs survey; [Matsuoka et al. 2016](#)) lie closer to the local relation confirms this bias (e.g., [Izumi et al. 2019, 2021](#)).

Moreover, the mass measurements at high redshifts suffer from significant uncertainties with possibly systematic biases. For instance, the \mathcal{M}_{BH} of flux-limited quasar sample might be systematically overestimated by the single-epoch virial estimator (e.g., [Vestergaard & Osmer 2009](#); hereafter VO09) because of uncorrelated variation between AGN luminosity and broad line width (especially for Mg II and C IV) that gives rise to a luminosity-dependent virial BH mass bias (hereafter the SE bias) as detailed in [Shen \(2013\)](#). In addition, the hosts of $z \sim 6$ quasars are found to be gas-rich (e.g., [Decarli et al. 2022](#)), thus approximating \mathcal{M}_\star by \mathcal{M}_{dyn} is likely an overestimate.

In this paper, we attempt to model the selection and measurement biases for a $z \sim 6$ quasar sample compiled in the literature in order to reveal the underlying connection between SMBH and galaxy growth in the early universe. This work assumes a cosmological model with $\Omega_\Lambda = 0.7$, $\Omega_m = 0.3$, and $H_0 = 70 \text{ km s}^{-1} \text{ Mpc}^{-1}$. All magnitudes are given in the AB system. The stellar mass and SFR are based on the [Chabrier \(2003\)](#) initial mass function (IMF).

2. SAMPLE

We adopt the $z \sim 6$ quasar sample compiled in [Izumi et al. \(2021\)](#) as our parent sample. It contains 46 quasars with \mathcal{M}_{BH} , \mathcal{M}_{dyn} , quasar luminosity (L_{3000} and M_{1450}), and infrared (IR) luminosity measurements from the literature. The \mathcal{M}_{BH} of 22/46 objects are derived from the virial estimator using the VO09 calibration for the Mg II line as

$$\log\left(\frac{\mathcal{M}_{\text{BH}}}{M_\odot}\right) = 6.86 + 0.5 \log\left(\frac{\lambda L_{\lambda 3000}}{10^{44} \text{ erg s}^{-1}}\right) + 2 \log\left(\frac{\text{FWHM}_{\text{Mg II}}}{\text{km s}^{-1}}\right), \quad (1)$$

while Eddington-limited accretion is assumed to estimate the mass for the remaining 24 objects. The total IR luminosity (L_{TIR}) is derived by fitting the 1.2 mm ALMA continuum with an optically thin graybody spectrum assuming a dust temperature of 47 K and a dust spectral emissivity index of 1.6 that have been widely adopted for $z \sim 6$ quasars, then extrapolating to the total IR (8 – 1000 μm) range. The SFR is derived using $3.88 \times 10^{-44} L_{\text{TIR}}$ (multiplied by 0.94 to convert to the [Chabrier \(2003\)](#) IMF; [Murphy et al. 2011](#)), assuming that the cold interstellar medium is predominantly heated by star formation. The dynamical masses \mathcal{M}_{dyn} of these quasars are derived through gas kinematics using the [C II] line. The standard rotating thin disk approximation is assumed for all quasars except two (given as upper limits). In this work, we only consider the 20 objects whose \mathcal{M}_{BH} and \mathcal{M}_{dyn} are derived from the Mg II line and the rotating thin disk assumption, respectively, to ensure relatively reliable mass measurements. However, we caution that the derived \mathcal{M}_{dyn} is highly sensitive to the assumptions made on galaxy geometry and inclination angle (e.g., [Wang et al. 2013](#)).

Ignoring the contribution of dark matter within the galaxy, we estimate the \mathcal{M}_\star of these quasars by subtracting the expected molecular gas mass (\mathcal{M}_{gas}) from their total \mathcal{M}_{dyn} , assuming that quasar hosts have similar gas content as star forming galaxies (e.g., [Molina et al. 2021](#)). We adopt the typical $\mathcal{M}_{\text{gas}}/\mathcal{M}_\star$ ratio (μ_{gas}) of $z \sim 6$ galaxies given by [Tacconi et al. \(2018\)](#):

$$\log \mu_{\text{gas}} = 0.12 - 3.62 \times (\log(1+z) - 0.66)^2 - 0.35 \times (\log \mathcal{M}_\star - 10.7),$$

where we adopted their $\beta = 2$ result with the [Speagle et al. \(2014\)](#) star formation main sequence (MS) and assumed $\delta\text{MS} = 0$. We then use this relationship to estimate the typical \mathcal{M}_{gas} at a given \mathcal{M}_\star and derive the correlation between \mathcal{M}_\star and \mathcal{M}_{dyn} , where \mathcal{M}_{dyn} is approximated by $\mathcal{M}_\star + \mathcal{M}_{\text{gas}}$. The resulting \mathcal{M}_{gas} and

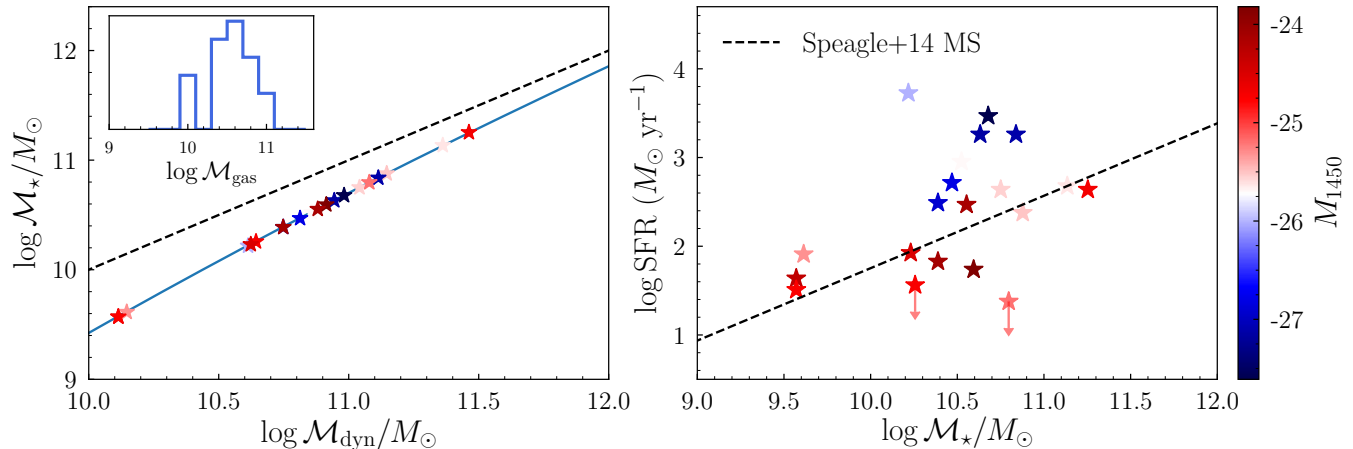


Figure 1. Left: Estimating stellar masses of $z \sim 6$ quasars by subtracting the expected molecular gas masses (inset histogram) from their dynamical masses. Quasars are plotted as stars color-coded by their M_{1450} . The blue curve shows the M_* – M_{dyn} relation derived from the M_{gas}/M_* vs. M_* relation given by [Tacconi et al. \(2018\)](#). The black dashed line shows the one-to-one relation. Right: The SFR– M_* plane of our quasars compared to the [Speagle et al. \(2014\)](#) main sequence relation at $z \sim 6$. Two objects with upper limits in SFR are marked by red arrows.

M_* of our quasars at their respective M_{dyn} are shown in Figure 1 (left panel). The gas mass is distributed between $\sim 10^{10} - 10^{11} M_{\odot}$, which is consistent with recent direct measurements in $z \sim 6$ quasars (e.g., [Decarli et al. 2022](#)). The derived M_* is typically 0.2–0.5 dex smaller than M_{dyn} . We also show the distribution of our quasars in the SFR – M_* plane in Figure 1 (right panel). As can be seen, most quasars are located near the [Speagle et al. \(2014\)](#) MS.

3. EVOLUTION OF THE $M_{\text{BH}} - M_*$ RELATION

3.1. The Observed $M_{\text{BH}} - M_*$ Relation

Figure 2 plots the $z \sim 6$ quasars in the $M_{\text{BH}} - M_*$ plane compared to the local $M_{\text{BH}} - M_{\text{bulge}}$ relation. We adopt the local relation given by [Häring & Rix \(2004\)](#) (HR04) to be self-consistent with the VO09 virial estimator (see Section 6.2 in [Ding et al. 2020](#) for the discussion on the choice of the local baseline). The local sample is consist of massive ellipticals and bulge-dominated S0 galaxies, thus we adopt $M_{\text{bulge}} \approx M_*$ in the following analyses. This figure confirms that quasars at $z \sim 6$ typically lie above the local relation, and the offset at a given stellar mass ($\Delta \log M_{\text{BH}}$) generally increases with quasar luminosity.

3.2. Estimating Expected Biases

As introduced in Section 1, the current $z \sim 6$ quasar sample suffers strong selection biases. Following [Li et al. \(2021\)](#), we perform a simple Monte Carlo simulation to build a mock AGN sample that mimics the observational biases as much as possible to account for such an effect in order to reveal the connection between the largely undetected SMBHs and their host galaxies. In the fol-

lowing, we briefly introduce our simulation method. The details of each step and the choice of model parameters are described in the Appendix A.

Our simulation starts with the galaxy stellar mass function (SMF) at $z \sim 6$ given by [Grazian et al. \(2015\)](#) and the $M_{\text{BH}} - M_*$ relation to generate a sample of mock galaxies and SMBHs. The $M_{\text{BH}} - M_*$ relation is assumed to have a gaussian intrinsic scatter (σ_{μ}) with a mean that evolves as

$$\Delta \log M_{\text{BH}} = \gamma \log(1+z). \quad (2)$$

Assuming that type 1 AGNs follow the same $M_{\text{BH}} - M_*$ relation as the underlying galaxy population (but see [Schulze & Wisotzki 2014](#) and also [Li et al. 2021](#)), we convert the mass of each simulated SMBH to bolometric luminosity by adopting an intrinsic Eddington ratio (λ_{Edd}) distribution function (ERDF) of type 1 AGNs. We adopt the ERDF at $z = 4.75$ given by [Kelly & Shen \(2013\)](#) who jointly constrained the intrinsic ERDF and the active BH mass function (BHMF) based on uniformly-selected SDSS quasars with the sample incompleteness being carefully corrected in a Bayesian framework.

We then derive a virial M_{BH} for each mock AGN using the VO09 virial estimator based on its true M_{BH} , luminosity, an assumed FWHM distribution (in a log-normal form; [Shen 2013](#)), and a parameter β ($0 \leq \beta \leq 1$) that describes the fraction of correlated response of line width to the variation of luminosity. We adopt $\beta = 0.6$ in this work; $\beta \neq 1$ will give rise to the SE bias ([Shen 2013](#)). The resulting virial M_{BH} has a 0.4 dex scatter relative to the true M_{BH} and it tends to overestimate the true M_{BH} if $L > \bar{L}$ (and vice versa), where L is the

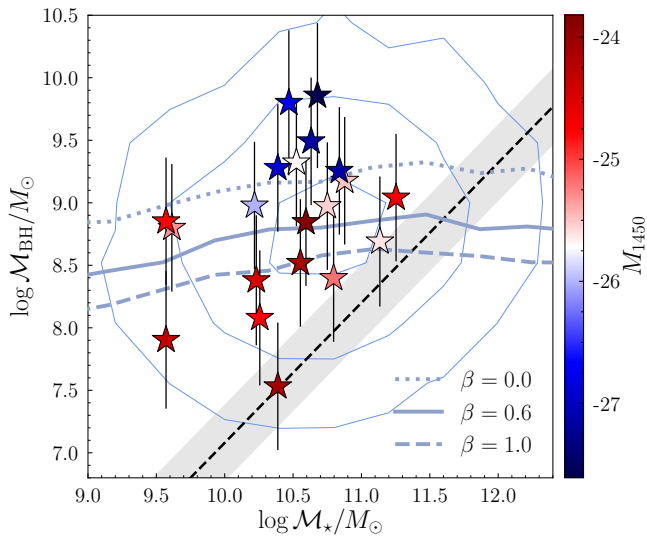


Figure 2. The $\mathcal{M}_{\text{BH}} - \mathcal{M}_*$ distribution at $z \sim 6$. The individual points show the observed quasars color-coded by their M_{1450} . The blue contours show the mock AGN sample which mimics the selection function and measurement uncertainties of observations (i.e., Mock-Q) assuming $\beta = 0.6$. The average $\mathcal{M}_{\text{BH}} - \mathcal{M}_*$ relations of the mock AGN samples generated from $\beta = 0.0$, 0.6 , and 1.0 are plotted as dotted, solid, and dashed blue curves, respectively. The local HR04 relation and its scatter are shown as a black dashed line and a gray shaded region, respectively.

luminosity of an AGN with a true BH mass of $\mathcal{M}_{\text{BH,true}}$, and \bar{L} is the average luminosity of all AGNs at the same $\mathcal{M}_{\text{BH,true}}$ (see Appendix A for details). In addition, we add a random gaussian error with a dispersion of 0.5 dex to each true \mathcal{M}_* to reflect the large uncertainties of estimating \mathcal{M}_* from \mathcal{M}_{dyn} .

In our framework, under the assumption of no evolution in the $\mathcal{M}_{\text{BH}} - \mathcal{M}_*$ relation (i.e., $\gamma = 0.0$, $\sigma_\mu = 0.3$) of the underlying SMBH populations, one can estimate the expected bias (i.e., a positive $\Delta \log \mathcal{M}_{\text{BH}}$ relative to the local relation) caused by the sample selection function by applying the same selection criteria of observations to mock AGNs. However, it is infeasible to define a selection function as our sample is a mixture of $z \sim 6$ quasars from various surveys with additional requirements of having near-IR spectroscopic and ALMA follow up to measure \mathcal{M}_{BH} and \mathcal{M}_{dyn} . Therefore, we assume a simplified scenario that all the selection biases come from the “effective” magnitude limit of different surveys, where effective means that these quasars are the relatively luminous ones selected from their parent samples for follow up observations. We simulate this selection function by producing randomly drawn samples of mock quasars that are matched to the observed M_{1450} distribution (hereafter the Mock-Q sample).

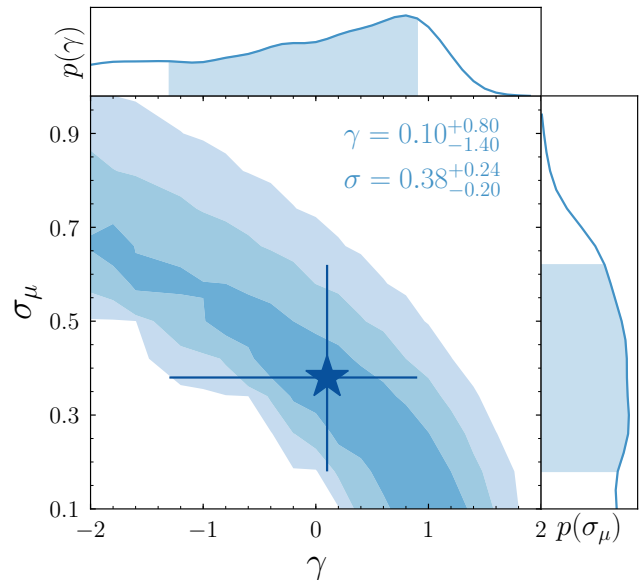


Figure 3. An example of constraining the evolution factor γ and the intrinsic scatter σ_μ based on a specific model ($\beta = 0.6$). The contours represent the $1\sigma - 3\sigma$ confidence regions of the posterior probability. The histograms are the marginalized posterior distributions. The star indicates the posterior median and its 1σ error.

The distribution of the Mock-Q sample in the $\mathcal{M}_{\text{BH}} - \mathcal{M}_*$ plane is shown as blue contours in Figure 2. The virial \mathcal{M}_{BH} tends to overestimate the true \mathcal{M}_{BH} by ~ 0.25 dex in this case (see Figure 5e in the Appendix). Given the magnitude limit and the large uncertainties being added to both masses, the distribution is strongly modulated compared to the originally assumed HR04 relation. In Figure 2 we also show the average virial \mathcal{M}_{BH} in bins of \mathcal{M}_* for the Mock-Q sample. It represents the expected offset caused by selection effects and measurement uncertainties. To rephrase, any offset and large scatter in the observed $\mathcal{M}_{\text{BH}} - \mathcal{M}_*$ relation that follows these curve and contours could be considered as no significant evolution in the mass relation of the underlying SMBH populations, which appears to be true for our quasar sample.

We also test the impact of changing β (Figure 2). As a reference, assuming $\beta = 1.0$ (i.e., no SE bias) and $\beta = 0.0$ (i.e., the maximum SE bias for which the BH mass tends to be overestimated by ~ 0.65 dex) will cause systematic shifts of the average $\mathcal{M}_{\text{BH}} - \mathcal{M}_*$ relation of the Mock-Q sample by about $+0.2$ dex and -0.4 dex (relative to the $\beta = 0.6$ curve), respectively. In these cases, an evolving intrinsic $\mathcal{M}_{\text{BH}} - \mathcal{M}_*$ relation is required to explain the observed data points.

3.3. Constraining the Intrinsic $\mathcal{M}_{\text{BH}} - \mathcal{M}_*$ Relation

The fact that the observed offset can be reproduced by a non-evolving $\mathcal{M}_{\text{BH}} - \mathcal{M}_\star$ relation does not rule out other evolving models. Therefore, we further constrain the intrinsic evolution by generating mock AGNs with a range of γ and σ_μ (assuming $\beta = 0.6$) and comparing the resulting $\mathcal{M}_{\text{BH}} - \mathcal{M}_\star$ relation (incorporating observational biases) with the observed one to derive the likelihood (see Section 5 in Li et al. 2021 for details).

The posterior distributions of γ and σ_μ assuming a bounded flat prior ($-2.0 < \gamma < 2.0$, $\sigma_\mu > 0.1$) are shown in Figure 3. There is a strong degeneracy between γ and σ_μ : both a positive evolution (i.e., $\mathcal{M}_{\text{BH}}/\mathcal{M}_\star$ increases with redshift) with a small σ_μ , or even a negative evolution with a large σ_μ can reproduce the large apparent offset. The peak of the posterior distribution is somewhat skewed towards a positive evolution with a small scatter, as the current sample only probes overmassive quasars that are clustered at the top left of the local relation. The best-fit values based on the 16th, 50th, and the 84th percentiles of the marginalized posterior distributions are $\gamma = 0.10^{+0.80}_{-1.40}$ and $\sigma_\mu = 0.38^{+0.24}_{-0.20}$, which could be consistent with a non-evolving $\mathcal{M}_{\text{BH}}/\mathcal{M}_\star$ out to $z \sim 6$ (Volonteri & Stark 2011; Schulze & Wisotzki 2014).

However, given various systematic uncertainties related to mass measurements and model assumptions, it is improper to interpret the complex evolution with a single number based on a certain model. For instance, the simplified thin-disk approximation will yield an underestimated \mathcal{M}_{dyn} (thus \mathcal{M}_\star) if the galaxy contains a dispersion-dominated component (e.g., Pensabene et al. 2020). In addition, while we intended to use the total \mathcal{M}_\star of these quasars in our analysis which has been shown to correlate better with \mathcal{M}_{BH} than using $\mathcal{M}_{\text{bulge}}$ at high redshifts (e.g., Jahnke et al. 2009; Schramm & Silverman 2013; Li et al. 2021), the [C II] emission line mainly traces the inner galaxy region but not the entire galaxy (e.g., Venemans et al. 2017). These effects, together with the very uncertain gas fraction and the choice of β can all induce systematic shifts of the mass measurements and affect the posterior distributions. Moreover, the bias estimates also depend on the assumed underlying distribution functions (e.g., the ERDF), which are not well-constrained at $z \sim 6$ (see Section 6.3 in Li et al. 2021 for a detailed discussion). Therefore, it is clear that the current dataset is insufficient to robustly constrain the intrinsic $\mathcal{M}_{\text{BH}} - \mathcal{M}_\star$ relation of the underlying SMBH populations at $z \sim 6$.

3.4. Predicted Evolution in the $\mathcal{M}_{\text{BH}} - \mathcal{M}_\star$ Plane

Although the intrinsic evolution of the underlying SMBH populations is unclear, overmassive quasars do

exist. It is inevitable that their vigorous BH growth needs to be inhibited at some point in order to avoid unreasonably large \mathcal{M}_{BH} and to prevent them from being further deviate from the local relation where they eventually end up. The future positions of these quasars in the $\mathcal{M}_{\text{BH}} - \mathcal{M}_\star$ plane can be traced under the measured instantaneous BH accretion rate (BHAR) and SFR (e.g., Venemans et al. 2016). The BHAR can be estimated as

$$\dot{\mathcal{M}}_{\text{BH}} = \frac{(1 - \eta) L_{\text{bol}}}{\eta c^2}, \quad (3)$$

where $\eta = 0.1$ (e.g., Trakhtenbrot et al. 2017) is the assumed radiative efficiency that is suitable for our moderately accreting SMBHs (80% of our sample have $-1 < \log \lambda_{\text{Edd}} \lesssim 0$), and c is the speed of light. We assume that these $z \sim 6$ quasars can continue to form stars at their current SFR for a period (Δt). At the same time, the SMBHs keep accreting at the measured BHAR for a fraction of this time (i.e., the AGN duty cycle). It is challenge to constrain how long a quasar can sustain its high accretion rate with recent studies reported a short quasar lifetime at $z \sim 6$ ($\sim 10^6$ yrs on average; Eilers et al. 2021). We estimate the \mathcal{M}_{BH} -dependent duty cycle by approximating it with the active SMBH fraction (see the inset in Figure 4), which is derived from the ratio between the BHMF of type 1 AGNs at $z \sim 4.75$ given by Kelly & Shen (2013) to the total BHMF scaled from the Grazian et al. (2015) SMF at the same redshift assuming a $\mathcal{M}_{\text{BH}} - \mathcal{M}_\star$ relation with $\gamma = 0.1$ and $\sigma_\mu = 0.38$ (Section 3.3). We adopt Δt as the minimum value between the gas depletion timescale ($t_{\text{del}} = \mathcal{M}_{\text{gas}}/\text{SFR}$; $\sim 10 - 1000$ Myrs) and 100 Myrs. The assembled \mathcal{M}_{BH} and \mathcal{M}_\star during this period are illustrated by the dashed arrows in Figure 4.

Interestingly, the predicted evolution exhibits a flow pattern, where quasars that are significant outliers in $\mathcal{M}_{\text{BH}}/\mathcal{M}_\star$ tend to converge to the local relation as previously seen at $z < 2$ (e.g., Merloni et al. 2010; Sun et al. 2015). We also show the evolution vectors (see the solid arrows) after correcting the active fraction for type 2 AGNs (see the inset in Figure 4) assuming the luminosity-dependent obscured fraction ($\sim 60 - 80\%$ at $z \sim 6$) given by Vito et al. (2018) in order to account for the possible underestimate of the BH growth time that is not captured by the BHMF of type 1s. Still, the general trend remains. The converging pattern also holds if we adopt the peak value of γ and σ_μ when estimating the total BHMF which results in lower AGN duty cycles. A natural explanation of the flow pattern could be AGN feedback, which suppresses the growth of SMBHs once they deviate significantly from the local relation.

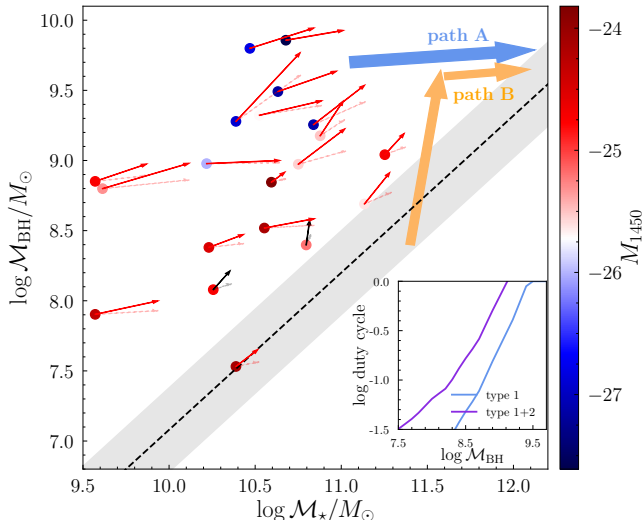


Figure 4. The predicted evolution of the growth of SMBHs and their host galaxies in the next $\min(t_{\text{del}}, 100)$ Myrs. The dashed arrows represent the evolution vectors assuming the AGN duty cycle derived from the type 1 BHMF, while the solid arrows show the evolution vectors after correcting the duty cycle for type 2 AGNs. Two objects with upper limits in SFR are shown as black (gray) arrows. The adopted duty cycle – \mathcal{M}_{BH} relations are shown in the inset. The blue and orange arrows show the possible evolution pathways for overmassive quasars. The black dashed line and the shaded region represent the local HR04 relation and its scatter, respectively.

The converging pattern for the most luminous and massive BHs may suggest that they have experienced rapid accretion episodes in the seeding epochs and maintain being overmassive until reaching the local relation (i.e., path A in Figure 4) as shown by recent numerical simulations (e.g., Inayoshi et al. 2021). However, we can not rule out the possibility that their progenitors are low-mass BHs moving upwards at similar stellar masses (i.e., path B in Figure 4). Such low- \mathcal{M}_{BH} objects are undersampled in current surveys due to the detection limit, and their vigorous BH accretion may occur rapidly in a highly obscured or/and a radiative inefficient mode which further reduces their apparent luminosity (e.g., Trebitsch et al. 2019; Davies et al. 2019). Therefore, it is essential to study the growth of low mass systems and obscured quasars that have recently been discovered at $z \sim 6$ (e.g., Onoue et al. 2021).

4. CONCLUDING REMARKS

The $z \sim 6$ quasars observed typically have $\mathcal{M}_{\text{BH}}/\mathcal{M}_*$ significantly larger than the local value. However, strong selection biases and significant measurement uncertainties severely limit the interpretation of the data. In this work, we demonstrated that once

these factors are considered, the large apparent offset and observed scatter could be fully reproduced by assuming that the underlying SMBH populations at $z \sim 6$ follow the local $\mathcal{M}_{\text{BH}} - \mathcal{M}_*$ relation (Figure 2). However, a positive or even a negative evolution can also explain the data well, depending on the evolution of the intrinsic scatter and various systematic uncertainties (Figure 3). It is thus crucial to emphasize that the evolution of the offset cannot be properly assessed without considering the scatter (see Li et al. 2021 for a similar issue at $z < 1$). Interestingly, quasars that are significant outliers in $\mathcal{M}_{\text{BH}}/\mathcal{M}_*$ tend to have evolution vectors pointing toward the local relation (Figure 4). This may provide tentative evidence that a self-regulated SMBH-galaxy coevolution scenario is already in place at $z \sim 6$, possibly driven by AGN feedback.

To break the degeneracy, expanding the current sample in both number statistics and to lower \mathcal{M}_{BH} limits are imperative (e.g., Habouzit et al. 2022). This is expected to be achieved by the ongoing SHELLQs survey and the forthcoming surveys by the Vera C. Rubin Observatory and Euclid, which will offer promisingly large and less-biased quasar samples with a more uniform selection function. It is also crucial to reduce the uncertainties (especially the systematic ones) in the mass measurements. The James Webb Space Telescope will enable us to measure \mathcal{M}_{BH} using the more reliable $\text{H}\beta$ line, and makes it possible to probe the stellar emissions of $z \sim 6$ quasars in the rest-frame optical bands thus allowing direct measurements of their \mathcal{M}_* . In the meantime, extending the current reverberation-mapped AGN sample to a wider parameter space is crucial to validate and improve the virial \mathcal{M}_{BH} estimator, which will be achieved by the ongoing SDSS-V Black Hole Mapper survey. These efforts, together with a deeper understanding of the AGN accretion process (e.g., radiative efficiency, duty cycle) will allow us to better assess the connection between SMBH and galaxy growth in the reionization era.

ACKNOWLEDGMENTS

J.D.S. is supported by the JSPS KAKENHI Grant Number JP18H01251, and the World Premier International Research Center Initiative (WPI Initiative), MEXT, Japan. K.I. acknowledges support from the National Natural Science Foundation of China (12073003, 12003003, 11721303, 11991052, 11950410493), the National Key R&D Program of China (2016YFA0400702), and the China Manned Space Project with NO. CMS-CSST-2021-A04 and CMS-CSST-2021-A06.

APPENDIX

A. DETAILS OF GENERATING A MOCK AGN SAMPLE

In this appendix we introduce the steps of our simulation by assuming $\gamma = 0.0$ and $\sigma_\mu = 0.3$ as an example. Our simulation starts with the SMF at $z \sim 6$ given by [Grazian et al. \(2015\)](#) to generate a sample of mock galaxies ranging from $8.0 < \log \mathcal{M}_*/M_\odot < 11.0$. We assume that the $\mathcal{M}_{\text{BH}} - \mathcal{M}_*$ relation at $z \sim 6$ is the same as the local HR04 relation in terms of both mean and intrinsic scatter, and randomly assign each mock galaxy a *true* \mathcal{M}_{BH} based on the HR04 relation. The resulting $\mathcal{M}_{\text{BH}} - \mathcal{M}_*$ distribution is shown in blue in Figure 5a.

We convert \mathcal{M}_{BH} into bolometric luminosity by randomly sampling the intrinsic ERDF given by [Kelly & Shen \(2013\)](#) at $z = 4.75$ in the range of $-1.5 < \log \lambda_{\text{Edd}} < 0.5$ ([Shen et al. 2019](#); [Onoue et al. 2019](#)). The bolometric luminosity is converted into rest-frame luminosity L_{3000} and absolute magnitude M_{1450} (Figure 5b) assuming the bolometric corrections to be 5.15 and 4.4, respectively ([Richards et al. 2006](#)). After these steps, we have the full knowledge of the *true* distribution of mock AGNs in the $\mathcal{M}_* - \mathcal{M}_{\text{BH}} - L$ plane.

We then add realistic uncertainties to the mass terms to resemble observations. Given the large uncertainties on \mathcal{M}_{dyn} and \mathcal{M}_{gas} , we first add a random gaussian uncertainty with a standard deviation of 0.5 dex to each true \mathcal{M}_* (Figure 5c). We also derive a virial \mathcal{M}_{BH} for each mock AGN using their true \mathcal{M}_{BH} , L_{3000} , and an assumed Mg II FWHM distribution through Equation 1. In this step, we take into account the luminosity-dependent SE bias.

The SE bias originates from uncorrelated scatter between AGN luminosity and emission line width due to both the variability of individual quasar and the object-by-object diversity in the broad-line region (BLR) properties at a fixed true \mathcal{M}_{BH} ([Shen 2013](#)). We consider the following cases to represent different levels of the SE bias:

- Case A: the virial \mathcal{M}_{BH} is an unbiased estimator of the true \mathcal{M}_{BH} regardless of AGN luminosity. This is done by assuming that the FWHM of Mg II follows a log-normal distribution ([Shen et al. 2011](#)) with the mean value determined by the *true* \mathcal{M}_{BH} and L_{3000} for each mock AGN using Equation 1. We randomly sample the log-normal distribution with a dispersion of σ_{FWHM} to generate FWHM for each source. The sampled FWHM is then combined with L_{3000} to derive virial \mathcal{M}_{BH} . The dispersion σ_{FWHM} is chosen such that the resulting scatter of virial \mathcal{M}_{BH} to true \mathcal{M}_{BH} is 0.4 dex. By doing so, the variation of luminosity (relative to the mean) at a fixed true \mathcal{M}_{BH} is compensated by the concordant variation in FWHM.
- Case B: Part of the variation in luminosity can be compensated by line width. To simulate such a situation, for each mock AGN, we derive the difference (ΔL) between its luminosity (L) and the mean luminosity (\bar{L}) for all mock AGNs of the same true \mathcal{M}_{BH} . We assume that a fraction (β) of ΔL can be compensated by line width, by using $\bar{L} + \beta \Delta L$ to determine the mean of the log-normal FWHM distribution for each source. In this case, the higher (lower)-than-the-mean luminosity can only be partly compensated by the lower (higher)-than-the-mean line width, thus the resulting virial \mathcal{M}_{BH} tends to overestimate (underestimate) the true \mathcal{M}_{BH} except at $L = \bar{L}$.

It is currently unclear how strong β is. The non-breathing effect of Mg II (i.e., the broad line width does not respond to the continuum variability in individual quasar) suggests that β is not one (e.g., [Yang et al. 2020](#)). However, despite the lack of a BLR size (R) – L relation for individual quasar (in case of Mg II), a global $R - L$ relation for a population of quasars spanning a broad range in BH masses and luminosities may still exist (e.g., [Homayouni et al. 2020](#)). This justifies the foundation of using the Mg II line as a single-epoch virial estimator, thus β is not likely to be zero. We adopt a relatively high response fraction ($\beta = 0.6$) as our fiducial model. This assumption yields $\Delta \log \text{FWHM}_{\text{Mg II}} \propto -0.15 \Delta L_{3000}$, as expected if the slope of the $R - L$ relation for Mg II is ~ 0.3 (e.g., [Homayouni et al. 2020](#)). The resulting FWHM distribution and the virial \mathcal{M}_{BH} vs. true \mathcal{M}_{BH} relation are shown in Figures 5d and 5e, respectively.

With the aforementioned steps, we have generated \mathcal{M}_* and virial \mathcal{M}_{BH} for each mock AGN with realistic uncertainties (Figure 5f). In Figure 5 we show the distributions of a mock AGN sample that matches with the observed M_{1450} distribution of $z \sim 6$ quasars in red. The originally assumed underlying distributions are strongly modulated by the magnitude limit and the large uncertainties on both masses.

REFERENCES

- Chabrier, G. 2003, PASP, 115, 763, doi: [10.1086/376392](https://doi.org/10.1086/376392)
- Davies, F. B., Hennawi, J. F., & Eilers, A.-C. 2019, ApJL, 884, L19, doi: [10.3847/2041-8213/ab42e3](https://doi.org/10.3847/2041-8213/ab42e3)

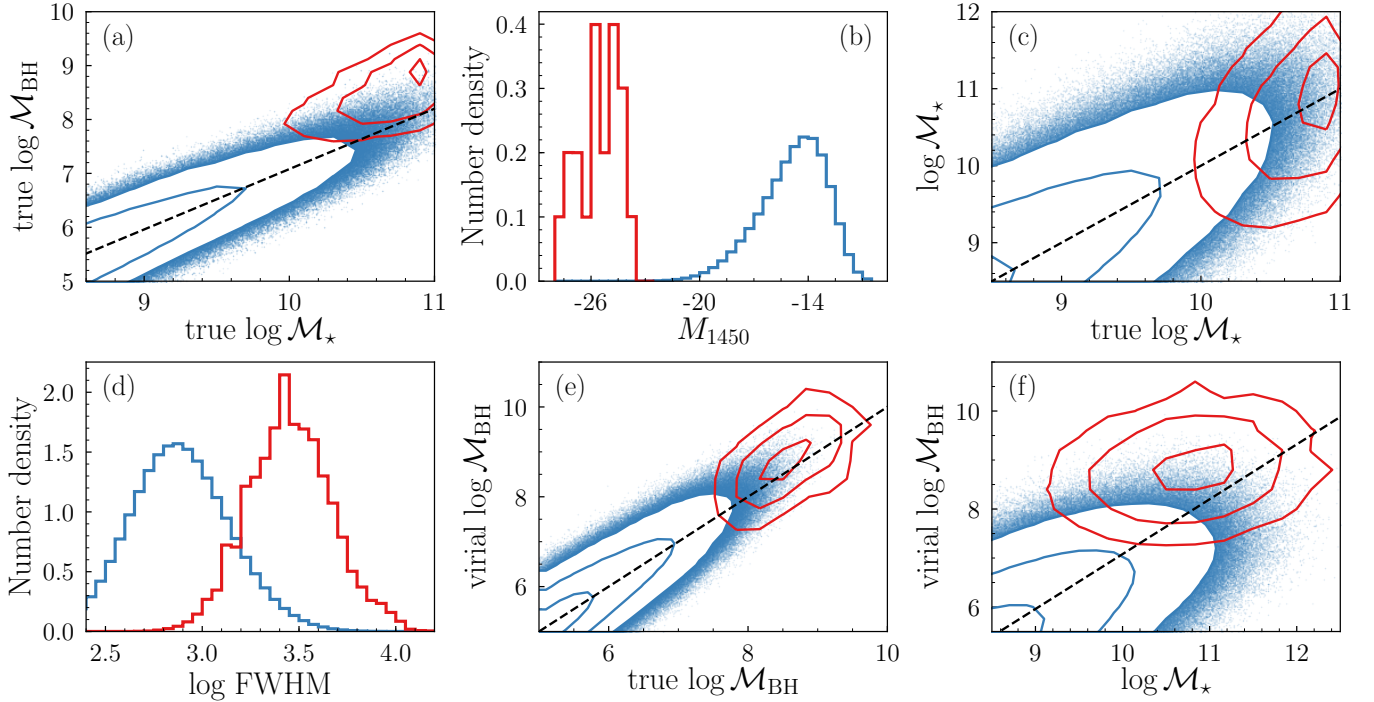


Figure 5. Parameter distributions of the mock AGN sample. The full mock sample is shown in blue. The mock sample that is matched in M_{1450} with the observed $z \sim 6$ quasar sample is shown in red.

Decarli, R., Pensabene, A., Venemans, B., et al. 2022, arXiv e-prints, arXiv:2203.03658.

<https://arxiv.org/abs/2203.03658>

Ding, X., Silverman, J., Treu, T., et al. 2020, ApJ, 888, 37, doi: [10.3847/1538-4357/ab5b90](https://doi.org/10.3847/1538-4357/ab5b90)

Eilers, A.-C., Hennawi, J. F., Davies, F. B., & Simcoe, R. A. 2021, arXiv e-prints, arXiv:2106.04586.

<https://arxiv.org/abs/2106.04586>

Fan, X., White, R. L., Davis, M., et al. 2000, AJ, 120, 1167, doi: [10.1086/301534](https://doi.org/10.1086/301534)

Grazian, A., Fontana, A., Santini, P., et al. 2015, A&A, 575, A96, doi: [10.1051/0004-6361/201424750](https://doi.org/10.1051/0004-6361/201424750)

Habouzit, M., Onoue, M., Bañados, E., et al. 2022, MNRAS, 511, 3751, doi: [10.1093/mnras/stac225](https://doi.org/10.1093/mnras/stac225)

Håring, N., & Rix, H.-W. 2004, ApJL, 604, L89, doi: [10.1086/383567](https://doi.org/10.1086/383567)

Homayouni, Y., Trump, J. R., Grier, C. J., et al. 2020, ApJ, 901, 55, doi: [10.3847/1538-4357/ababa9](https://doi.org/10.3847/1538-4357/ababa9)

Inayoshi, K., Nakatani, R., Toyouchi, D., et al. 2021, arXiv e-prints, arXiv:2110.10693.

<https://arxiv.org/abs/2110.10693>

Inayoshi, K., Visbal, E., & Haiman, Z. 2020, ARA&A, 58, 27, doi: [10.1146/annurev-astro-120419-014455](https://doi.org/10.1146/annurev-astro-120419-014455)

Izumi, T., Onoue, M., Matsuoka, Y., et al. 2019, PASJ, 71, 111, doi: [10.1093/pasj/psz096](https://doi.org/10.1093/pasj/psz096)

Izumi, T., Matsuoka, Y., Fujimoto, S., et al. 2021, ApJ, 914, 36, doi: [10.3847/1538-4357/abf6dc](https://doi.org/10.3847/1538-4357/abf6dc)

Jahnke, K., Bongiorno, A., Brusa, M., et al. 2009, ApJL, 706, L215, doi: [10.1088/0004-637X/706/2/L215](https://doi.org/10.1088/0004-637X/706/2/L215)

Kelly, B. C., & Shen, Y. 2013, ApJ, 764, 45, doi: [10.1088/0004-637X/764/1/45](https://doi.org/10.1088/0004-637X/764/1/45)

King, A., & Pounds, K. 2015, ARA&A, 53, 115, doi: [10.1146/annurev-astro-082214-122316](https://doi.org/10.1146/annurev-astro-082214-122316)

Kormendy, J., & Ho, L. C. 2013, ARA&A, 51, 511, doi: [10.1146/annurev-astro-082708-101811](https://doi.org/10.1146/annurev-astro-082708-101811)

Lauer, T. R., Tremaine, S., Richstone, D., & Faber, S. M. 2007, ApJ, 670, 249, doi: [10.1086/522083](https://doi.org/10.1086/522083)

Li, J., Silverman, J. D., Ding, X., et al. 2021, ApJ, 922, 142, doi: [10.3847/1538-4357/ac2301](https://doi.org/10.3847/1538-4357/ac2301)

Matsuoka, Y., Onoue, M., Kashikawa, N., et al. 2016, ApJ, 828, 26, doi: [10.3847/0004-637X/828/1/26](https://doi.org/10.3847/0004-637X/828/1/26)

Merloni, A., Bongiorno, A., Bolzonella, M., et al. 2010, ApJ, 708, 137, doi: [10.1088/0004-637X/708/1/137](https://doi.org/10.1088/0004-637X/708/1/137)

Molina, J., Wang, et al. 2021, arXiv e-prints, arXiv:2101.00764. <https://arxiv.org/abs/2101.00764>

Murphy, E. J., Condon, J. J., Schinnerer, E., et al. 2011, ApJ, 737, 67, doi: [10.1088/0004-637X/737/2/67](https://doi.org/10.1088/0004-637X/737/2/67)

Neeleman, M., Novak, M., Venemans, B. P., et al. 2021, ApJ, 911, 141, doi: [10.3847/1538-4357/abe70f](https://doi.org/10.3847/1538-4357/abe70f)

Onoue, M., Kashikawa, N., Matsuoka, Y., et al. 2019, ApJ, 880, 77, doi: [10.3847/1538-4357/ab29e9](https://doi.org/10.3847/1538-4357/ab29e9)

Onoue, M., Matsuoka, Y., Kashikawa, N., et al. 2021, ApJ, 919, 61, doi: [10.3847/1538-4357/ac0f07](https://doi.org/10.3847/1538-4357/ac0f07)

- Pensabene, A., Carniani, S., Perna, M., et al. 2020, *A&A*, 637, A84, doi: [10.1051/0004-6361/201936634](https://doi.org/10.1051/0004-6361/201936634)
- Richards, G. T., Lacy, M., Storrie-Lombardi, L. J., et al. 2006, *ApJS*, 166, 470, doi: [10.1086/506525](https://doi.org/10.1086/506525)
- Schramm, M., & Silverman, J. D. 2013, *ApJ*, 767, 13, doi: [10.1088/0004-637X/767/1/13](https://doi.org/10.1088/0004-637X/767/1/13)
- Schulze, A., & Wisotzki, L. 2014, *MNRAS*, 438, 3422, doi: [10.1093/mnras/stt2457](https://doi.org/10.1093/mnras/stt2457)
- Shen, Y. 2013, *Bulletin of the Astronomical Society of India*, 41, 61. <https://arxiv.org/abs/1302.2643>
- Shen, Y., Richards, G. T., Strauss, M. A., et al. 2011, *ApJS*, 194, 45, doi: [10.1088/0067-0049/194/2/45](https://doi.org/10.1088/0067-0049/194/2/45)
- Shen, Y., Wu, J., Jiang, L., et al. 2019, *ApJ*, 873, 35, doi: [10.3847/1538-4357/ab03d9](https://doi.org/10.3847/1538-4357/ab03d9)
- Speagle, J. S., Steinhardt, C. L., Capak, P. L., & Silverman, J. D. 2014, *ApJS*, 214, 15, doi: [10.1088/0067-0049/214/2/15](https://doi.org/10.1088/0067-0049/214/2/15)
- Sun, M., Trump, J. R., Brandt, W. N., et al. 2015, *ApJ*, 802, 14, doi: [10.1088/0004-637X/802/1/14](https://doi.org/10.1088/0004-637X/802/1/14)
- Tacconi, L. J., Genzel, R., Saintonge, A., et al. 2018, *ApJ*, 853, 179, doi: [10.3847/1538-4357/aaa4b4](https://doi.org/10.3847/1538-4357/aaa4b4)
- Trakhtenbrot, B., Volonteri, M., & Natarajan, P. 2017, *ApJL*, 836, L1, doi: [10.3847/2041-8213/836/1/L1](https://doi.org/10.3847/2041-8213/836/1/L1)
- Trebitsch, M., Volonteri, M., & Dubois, Y. 2019, *MNRAS*, 487, 819, doi: [10.1093/mnras/stz1280](https://doi.org/10.1093/mnras/stz1280)
- Venemans, B. P., Walter, F., Zschaechner, L., et al. 2016, *ApJ*, 816, 37, doi: [10.3847/0004-637X/816/1/37](https://doi.org/10.3847/0004-637X/816/1/37)
- Venemans, B. P., Walter, F., Decarli, R., et al. 2017, *ApJ*, 837, 146, doi: [10.3847/1538-4357/aa62ac](https://doi.org/10.3847/1538-4357/aa62ac)
- Vestergaard, M., & Osmer, P. S. 2009, *ApJ*, 699, 800, doi: [10.1088/0004-637X/699/1/800](https://doi.org/10.1088/0004-637X/699/1/800)
- Vito, F., Brandt, W. N., Yang, G., et al. 2018, *MNRAS*, 473, 2378, doi: [10.1093/mnras/stx2486](https://doi.org/10.1093/mnras/stx2486)
- Volonteri, M., & Stark, D. P. 2011, *MNRAS*, 417, 2085, doi: [10.1111/j.1365-2966.2011.19391.x](https://doi.org/10.1111/j.1365-2966.2011.19391.x)
- Wang, R., Wagg, J., Carilli, C. L., et al. 2013, *ApJ*, 773, 44, doi: [10.1088/0004-637X/773/1/44](https://doi.org/10.1088/0004-637X/773/1/44)
- Yang, Q., Shen, Y., Chen, Y.-C., et al. 2020, *MNRAS*, 493, 5773, doi: [10.1093/mnras/staa645](https://doi.org/10.1093/mnras/staa645)